Journal of Biomechanics 92 (2019) 162–168

Contents lists available at ScienceDirect

Journal of Biomechanics

journal homepage: www.elsevier.com/locate/jbiomech
www.JBiomech.com

Short communication

Anatomically-based skeletal coordinate systems for use with impact biomechanics data intended for anthropomorphic test device development

Laura Slykhouse [a], Lauren Wood Zaseck [a,*], Carl Miller [a], John R. Humm [b], Aaron Alai [c], Yun Seok Kang [d], Chris Dooley [e], Don Sherman [f], Brian Bigler [g], Constantine K. Demetropoulos [e], Matthew P. Reed [a], Jonathan D. Rupp [h]

[a] University of Michigan Transportation Research Institute, United States
[b] Medical College of Wisconsin, United States
[c] United States Army Research Laboratory, United States
[d] The Ohio State University, United States
[e] John Hopkins University Applied Physics Laboratory, United States
[f] Wayne State University, United States
[g] Duke University, United States
[h] Emory University Department of Emergency Medicine, United States

ARTICLE INFO

Article history:
Accepted 21 May 2019

Keywords:
Local coordinate systems
Post-mortem human subjects
Impact testing
Instrumentation

ABSTRACT

Post-mortem human subjects (PMHS) are frequently used to characterize biomechanical response and injury tolerance of humans to various types of loading by means of instrumentation installed directly on the skeleton. Data extracted from such tests are often used to develop and validate anthropomorphic test devices (ATDs), which function as human surrogates in tests for injury assessment. Given that the location and orientation of installed instrumentation differs between subjects, nominally similar measurements made on different PMHS must be transformed to standardized, skeletal-based local coordinate systems (LCS) before appropriate data comparisons can be made. Standardized PMHS LCS that correspond to ATD instrumentation locations and orientations have not previously been published. This paper introduces anatomically-defined PMHS LCS for body regions in which kinematic measurements are made using ATDs. These LCS include the head, sternum, single vertebrae, pelvis, femurs (distal and proximal), and tibiae (distal and proximal) based upon skeletal landmarks extracted from whole body CT scans. The proposed LCS provide a means to standardize the reporting of PMHS data, and facilitate both the comparison of PMHS impact data across institutions and the application of PMHS data to the development and validation of ATDs.

1. Introduction

Post-mortem human subjects (PMHS) used to characterize the biomechanical response of humans to loading are typically instrumented with arrays of accelerometers and angular rate sensors mounted on the skeleton. Differences in installation procedures may yield inconsistencies in sensor location and orientation between subjects tested at different institutions. For example, different laboratories may use different hardware to install the sensors, resulting in variations in sensor location with respect to the bone (e.g., Bailey et al., 2015; Danelson et al., 2015; Kerrigan et al., 2008). Additionally, differences in subject anatomy can result in variations in sensor hardware location and orientation across different PMHS within a given test series. Given that sensor measurements are dependent on the location and orientation of the sensor on the skeleton, nominally similar measurements made on different PMHS must be transformed to standardized, skeleton-based local coordinate systems (LCS) to appropriately analyze the data.

Standardized LCS must fulfill specific criteria to be appropriate for the analysis and comparison of PMHS impact data. PMHS test data often support the development of anthropomorphic test devices (ATDs) that are used as human surrogates in physical

* Corresponding author.
E-mail address: laurekat@umich.edu (L.W. Zaseck).

https://doi.org/10.1016/j.jbiomech.2019.05.032
0021-9290/

testing. Examples include the Hybrid III (Foster et al., 1977) and THOR (Haffner et al., 2001) ATDs, which are validated for frontal impacts; the SID-IIs ATD (Daniel et al., 1995), which is validated for side impacts; and the WIAMan ATD, which is currently being validated for vertical acceleration impacts (Pietsch et al., 2016). Each of these ATDs has instrumentation at particular locations that can be defined relative to anatomic structures such as joint centers. For data from PMHS tests to be relatable to ATDs, PMHS instrumentation either needs to be installed in similar anatomic location as is used in ATDs or transformed from the measured location to the ATD instrumentation locations. Ideally, instrumentation is installed as close as possible to ATD measurement locations to minimize the noise that is introduced into signals from rigid body translations (Shaw et al., 2001), but few studies have attempted to define PMHS instrumentation locations in a manner that can be related to ATD measurements with minimal translation distance. Therefore, the two most important criteria that LCS must fulfill are that they are relatable to ATD measurements and located close to locations on the PMHS where sensors are typically installed.

Skeleton-based LCS currently described in the biomechanics literature are not fully appropriate for the analysis of PMHS impact data to serve ATD development. The most commonly used LCS (Grood and Suntay, 1983; Wu et al., 2002) were developed for reporting joint motion in clinically relevant terms based upon bony landmarks that are palpable or viewed from clinical radiographs. Such methods are error-prone (Chien et al., 2009; Holden et al., 1997), leading to inconsistently-defined LCS. Additionally, clinically-relevant LCS typically have origins near the ends of the bony structures (e.g., Yoshioka et al., 1987) or at the joint center of rotation (e.g., Wu et al., 2002), which are both prone to measurement errors (Stagni et al., 2000) and do not correlate well with ATD sensor locations. Other existing coordinate systems for the spine (Padgaonkar, 1976; Stokes, 1994; Wu et al., 2002), pelvis (White et al., 2009; Wu et al., 2002), and tibia (Grood and Suntay, 1983; Kerrigan et al., 2008; Pennock and Clark, 1990) are also generally not applicable to ATD sensor locations. This paper describes the development of anatomically-defined PMHS coordinate systems for body locations in which kinematic measurements are made using ATDs, including the head, sternum, single vertebra, pelvis, femurs (distal and proximal), and tibiae (distal and proximal). Since instrumented PMHS must undergo pre-test computed tomography (CT) scans to record the location and orientation of installed sensors, the LCS are based upon skeletal landmarks that can be consistently identified from CT images whether the specimen imaged is a whole body or a partial body. The proposed set of LCS was specifically developed to correspond with sensor locations on the Warrior Injury Assessment Manikin (WIAMan) ATD, currently being developed for injury assessment during vertical accelerative loading conditions (Pietsch et al., 2016) to aid in the comparison of PMHS and ATD biomechanical data.

2. Methods

2.1. Definitions of local coordinate systems

Each LCS is defined based upon bony landmarks from a pre-test CT scan of an instrumented PMHS, and presented in relation to 3-dimensional images of each relevant body region. The PMHS used for these illustrations was instrumented with six-degree-of-freedom (6DOF) sensors (Make: 6DX Pro, Manufacturer: Diversified Technical Systems, Inc.), which measured X-, Y- and Z-accelerations (Ax, Ay, and Az, respectively) and X-, Y- and Z-angular rotations (ARx, ARy, and ARz, respectively). The sensors were rigidly installed onto the PMHS skeleton, allowing the data to be relatable to ATD measurements (which are all based on skeletal forces, moments, accelerations, and angular velocities), and also avoids measurement errors that can occur when instrumentation is installed onto the skin (Benoit et al., 2006). Specifications regarding the PMHS used, instrumentation locations and installation, and CT scan specifics are included in Appendix I. The 6DOF sensors are also included in the images for reference (dotted rectangles).

2.1.1. Head

Anatomical landmarks of the skull (Fig. 1):

RT: Right Tragion
LT: Left Tragion
RIO: Right Orbit Inferior Margin
LIO: Left Orbit Inferior Margin
EAM: External Auditory Meatus (used if the tragions are not visible)

Definition of standard anatomical axes of the skull (Fig. 1):

Origin: The origin of the head coordinate system is located at the head center of gravity (**CG**), which is determined from the pretest CT scan by constructing separate 3-dimensional masks of the bone and flesh, and determining the weighted midpoint of the CG locations from each mask. Each mask has an assigned voxel density based on HU thresholds, and the CG is calculated based upon the mass weighted centroid of all voxels.
$\boldsymbol{Y_{head}}$: The line joining the left and right tragion pointing to the right. If the tragions are not visible, the left and right **EAM** may be used to define the axis.

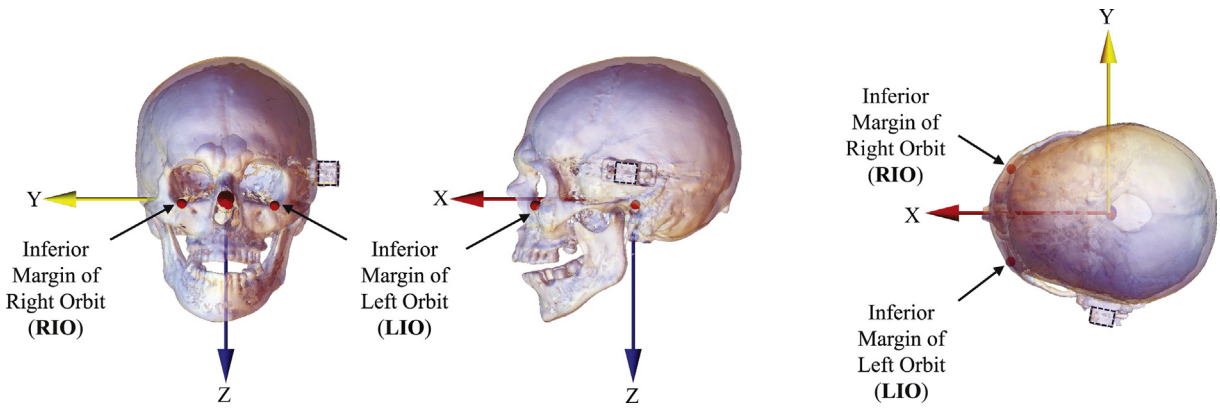

Fig. 1. Illustration of the head local coordinate system as defined by landmarks Inferior Margin of Right Orbit (**RIO**), and Inferior Margin of Left Orbit (**LIO**). Anterior (left), lateral (center), and superior (right) views shown. The installed 6 degree-of-freedom sensor block is visible on the lateral aspect of the left side of the skull.

$\boldsymbol{Z_{head}}$: The axis perpendicular to the line defined by connecting the midpoint of the left and right tragions to the midpoint of the interior margin of the **RIO** and **LIO** (i.e., **MIO**), perpendicular to $\boldsymbol{Y_{head}}$, pointing caudally.
$\boldsymbol{X_{head}}$: The line perpendicular to both $\boldsymbol{Y_{head}}$ and $\boldsymbol{Z_{head}}$, pointing anteriorly.

$$\boldsymbol{Y_{head}} = \frac{\mathbf{RT} - \mathbf{LT}}{|\mathbf{RT} - \mathbf{LT}|} \tag{1}$$

$$\boldsymbol{Z_{head}} = \frac{(\mathbf{MIO} - \mathbf{MT}) \times \boldsymbol{Y_{head}}}{|(\mathbf{MIO} - \mathbf{MT}) \times \boldsymbol{Y_{head}}|} \tag{2}$$

$$\boldsymbol{X_{head}} = \frac{\boldsymbol{Y_{head}} \times \boldsymbol{Z_{head}}}{|\boldsymbol{Y_{head}} \times \boldsymbol{Z_{head}}|} \tag{3}$$

2.1.2. Sternum

Anatomical landmarks of the sternum (Fig. 2):

JN: Jugular Notch
XPA: Anterior aspect of the Xiphoid Process Attachment
RR4: Right 4th Rib Attachment to sternum
LR4: Left 4th Rib Attachment to sternum

Definition of standard anatomical axes of the sternum (Fig. 2):

Origin: Located along $\boldsymbol{Z_{sternum}}$, positioned at the midpoint between the Z-components of **JN** and **XPA**.
$\boldsymbol{Z_{sternum}}$: The line parallel to the line connecting the **JN** and **XPA**, pointing caudally.
$\boldsymbol{X_{sternum}}$: The line perpendicular to $\boldsymbol{Z_{sternum}}$, and orthogonal to the line connecting the right and left 4th rib attachment points, pointing anteriorly.
$\boldsymbol{Y_{sternum}}$: The line perpendicular to both $\boldsymbol{X_{sternum}}$ and $\boldsymbol{Z_{sternum}}$, pointing to the right.

$$\boldsymbol{Z_{sternum}} = \frac{\mathbf{XPA} - \mathbf{JN}}{|\mathbf{XPA} - \mathbf{JN}|} \tag{4}$$

$$\boldsymbol{X_{sternum}} = \frac{(\mathbf{RR4} - \mathbf{LR4}) \times \boldsymbol{Z_{sternum}}}{|(\mathbf{RR4} - \mathbf{LR4}) \times \boldsymbol{Z_{sternum}}|} \tag{5}$$

$$\boldsymbol{Y_{sternum}} = \frac{\boldsymbol{Z_{sternum}} \times \boldsymbol{X_{sternum}}}{|\boldsymbol{Z_{sternum}} \times \boldsymbol{X_{sternum}}|} \tag{6}$$

2.1.3. Single vertebra

Anatomical landmarks of the single vertebra (Fig. 3):

LP: Left Pedicle
RP: Right Pedicle
SE: Area centroid of Superior Endplate
IE: Area centroid of Inferior Endplate
LTP: Lateral tip of the Left Transverse Process (not shown)
RTP: Lateral tip of the Right Transverse Process (not shown)

Definition of standard anatomical axes of the single vertebra (Fig. 3):

Origin: Located at the midpoint between the **SE** and **IE** landmarks.
$\boldsymbol{Y_{spine}}$: The line joining **LP** and **RP**, pointing to the right.
$\boldsymbol{X_{spine}}$: The line perpendicular to $\boldsymbol{Y_{spine}}$, and orthogonal to the line connecting the **SE** and **IE**, pointing anteriorly.
$\boldsymbol{Z_{spine}}$: The line perpendicular to both $\boldsymbol{X_{spine}}$ and $\boldsymbol{Y_{spine}}$, pointing caudally.

Note: The **SE** and **IE** landmarks may be determined by marking the perimeter of each end plate and then solving for their respective area centroids or calculated using software tools. If CT scan artifacts obscure **LP** or **RP**, the lateral tip of the left (**LTP**) and right transverse processes (**RTP**) may be used instead.

$$\boldsymbol{Y_{spine}} = \frac{\mathbf{RP} - \mathbf{LP}}{|\mathbf{RP} - \mathbf{LP}|} \tag{7}$$

$$\boldsymbol{X_{spine}} = \frac{\boldsymbol{Y_{spine}} \times (\mathbf{IE} - \mathbf{SE})}{|\boldsymbol{Y_{spine}} \times (\mathbf{IE} - \mathbf{SE})|} \tag{8}$$

$$\boldsymbol{Z_{spine}} = \frac{\boldsymbol{X_{spine}} \times \boldsymbol{Y_{spine}}}{|\boldsymbol{X_{spine}} \times \boldsymbol{Y_{spine}}|} \tag{9}$$

2.1.4. Pelvis

Anatomical landmarks of the pelvis (Fig. 4):

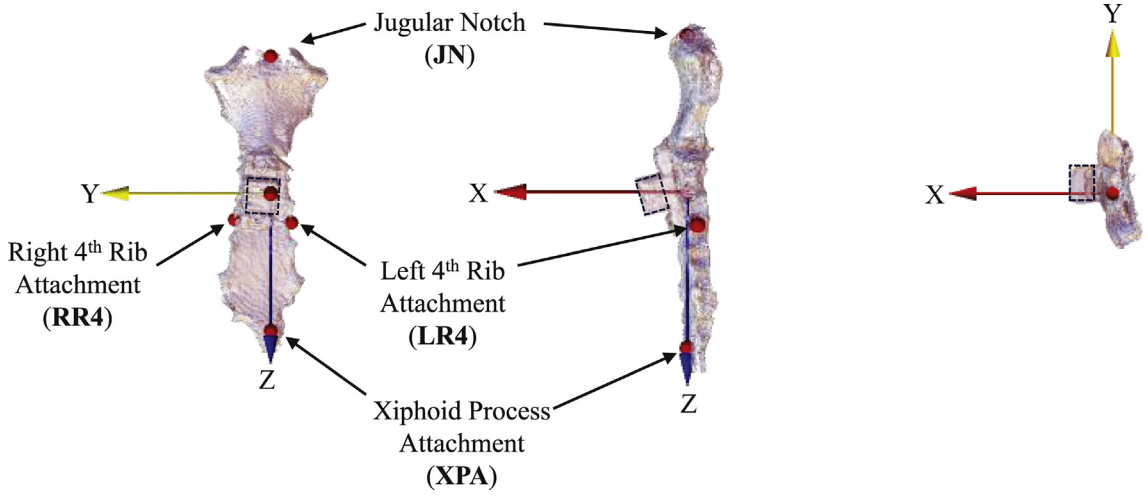

Fig. 2. Sternum local coordinate system as defined by landmarks Jugular Notch (**JN**), Xiphoid Process Attachment (**XPA**), Right 4th Rib attachment (**RR4**), and Left 4th Rib attachment (**LR4**). The sternum origin is located along $\boldsymbol{Z_{sternum}}$ and is positioned at the midpoint between the Z-components of the **JN** and **XPA** landmarks. Anterior (left), lateral (center), and superior (right) views shown. The installed 6 degree-of-freedom sensor block is visible, centered on the anterior aspect of the sternum.

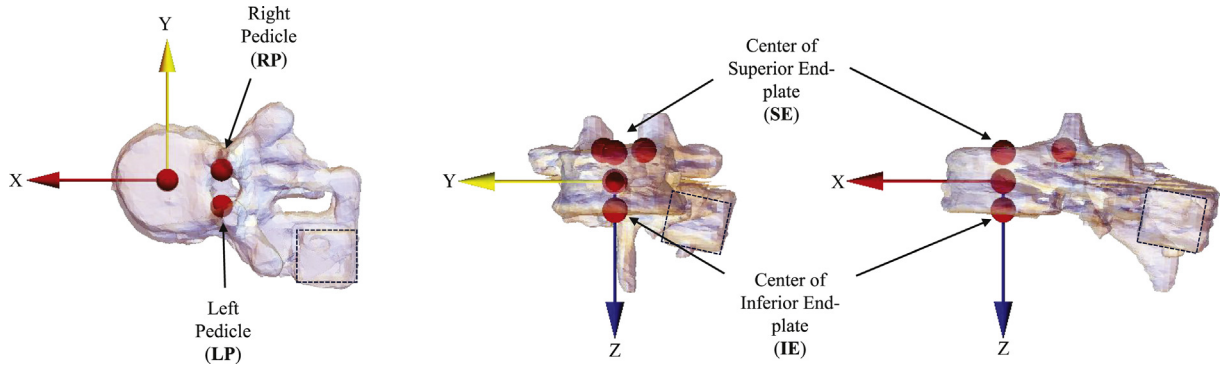

Fig. 3. Illustration of the vertebral local coordinate system as defined by landmarks Left Pedicle (**LP**), Right Pedicle (**RP**), center of Superior Endplate (**SE**), and center of Inferior Endplate (**IE**). The origin of the vertebrae is located along $\boldsymbol{Z_{spine}}$ and is positioned at the midpoint between **SE** and **IE**. Anterior (left), lateral (center), and superior (right) views shown. The installed 6 degree-of-freedom sensor block is visible posterior to the vertebral body.

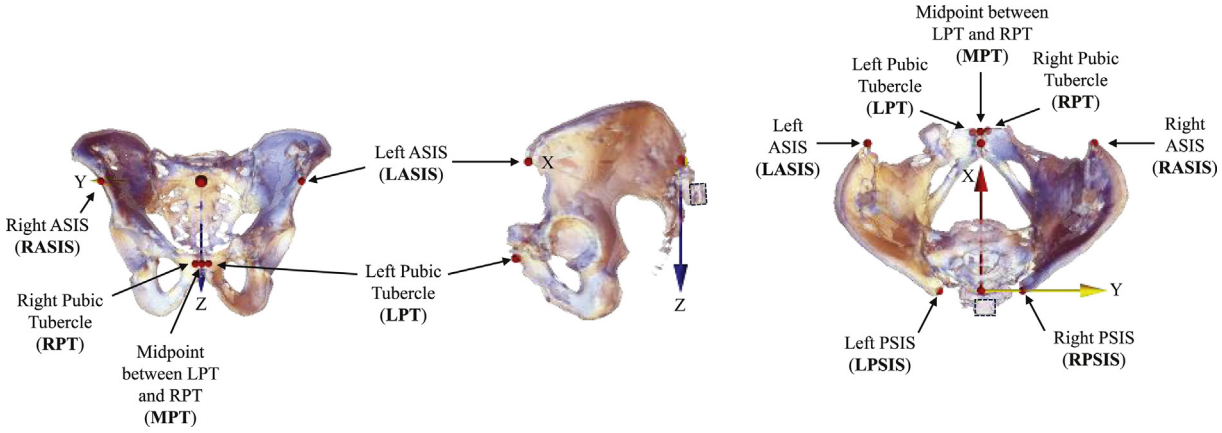

Fig. 4. Illustration of the pelvis local coordinate system as defined by landmarks Right ASIS (**RASIS**), Left ASIS (**LASIS**), Right PSIS (**RPSIS**), Left PSIS (**LPSIS**), Right Pubic Tubercle (**RPT**), and Left Pubic Tubercle (**LPT**), and the calculated landmark Mid Pubic Tubercle (**MPT**). Anterior (left), lateral (center), and superior (right) views shown. The installed 6 degree-of-freedom sensor block is visible on the on the posterior surface of the sacrum.

RASIS: Right ASIS
LASIS: Left ASIS
RPSIS: Right PSIS
LPSIS: Left PSIS
RPT: Right Pubic Tubercle
LPT: Left Pubic Tubercle
MASIS: Midpoint between the right and left ASIS
MPSIS: Midpoint between the right and left PSIS
MPT: Midpoint between the right and left Pubic Tubercle

Definition of standard anatomical axes of the pelvis (Fig. 4):

Origin: The origin for instrumentation installed on the sacrum is located at **MPSIS**. If instrumentation is installed near the pubic symphysis, its origin should be located at **MPT**. If additional instrumentation is installed on either iliac wing, the installed sensor location should be used as their origin.
$\boldsymbol{Y_{pelvis}}$: The line joining the right and left **ASIS**, pointing to the right.
$\boldsymbol{Z_{pelvis}}$: The line perpendicular to $\boldsymbol{Y_{pelvis}}$ and the line that joins the midpoint of the **ASIS** and **PSIS**, pointing caudally.
$\boldsymbol{X_{pelvis}}$: The line perpendicular to both $\boldsymbol{Y_{pelvis}}$ and $\boldsymbol{Z_{pelvis}}$, pointing anteriorly.

$$\boldsymbol{Y_{pelvis}} = \frac{\mathbf{RASIS} - \mathbf{LASIS}}{|\mathbf{RASIS} - \mathbf{LASIS}|} \tag{10}$$

$$\boldsymbol{Z_{pelvis}} = \frac{(\mathbf{MASIS} - \mathbf{MPSIS}) \times \boldsymbol{Y_{pelvis}}}{|(\mathbf{MASIS} - \mathbf{MPSIS}) \times \boldsymbol{Y_{pelvis}}|} \tag{11}$$

$$\boldsymbol{X_{pelvis}} = \frac{\boldsymbol{Y_{pelvis}} \times \boldsymbol{Z_{pelvis}}}{|\boldsymbol{Y_{pelvis}} \times \boldsymbol{Z_{pelvis}}|} \tag{12}$$

2.1.5. Femur

Both proximal and distal LCS are proposed on the femurs. Anatomical landmarks of the femur (Fig. 5):

LFE: Lateral Femoral Epicondyle
MFE: Medial Femoral Epicondyle
AFE: Average Femoral Epicondyle
FHC: Femoral Head Center

Note: Landmark **FHC** is calculated by sectioning the femoral head at the neck (by inspection) and performing a least-squares sphere fit. **FHC** is located at the center of this sphere. Landmark **AFE** is located at the midpoint between **LFE** and **MFE**.

Definition of standard anatomical axes of the femur (Fig. 5):

Origin: The Proximal Femur Origin and Distal Femur Origin are located along $\boldsymbol{Z_{femur}}$ at distances from **FHC** equal to 25% and 75% of the length of the femur (ℓ_{femur}) as defined by the difference between the z-components of **FHC** and **AFE**.

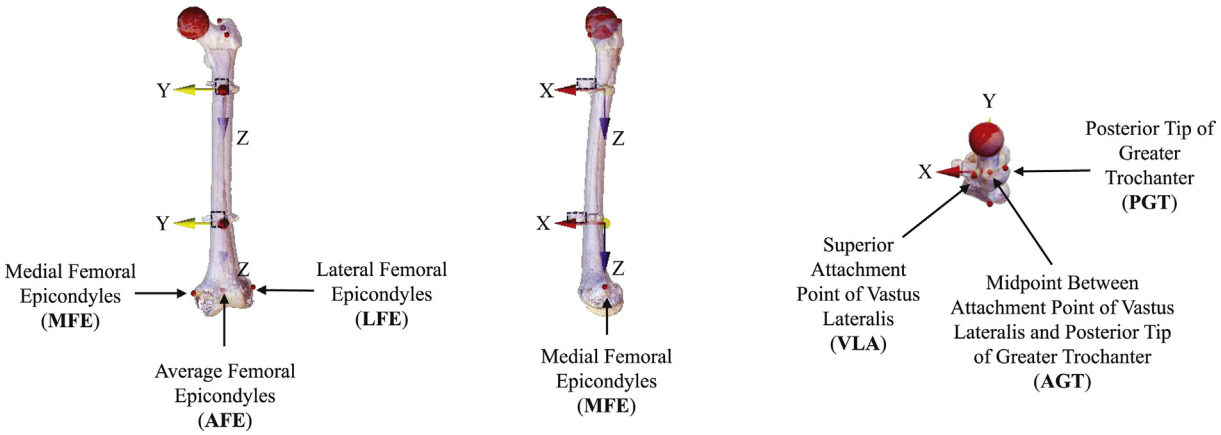

Fig. 5. Illustration of the local femur coordinate system as defined by the digitized landmarks Lateral Femoral Epicondyle (**LFE**) and Medial Femoral Epicondyle (**MFE**), and the calculated landmarks Center of Femoral Head (**FHC**) and Average Femoral Epicondyle (**AFE**). Anterior (left), lateral (center), and superior (right) views shown. The installed 6 degree-of-freedom sensor blocks are visible on the anterior surface of the distal and proximal femoral shaft.

$\boldsymbol{Z_{femur}}$: The line connecting the center of the femoral head to the average femoral epicondyle, pointing caudally.
$\boldsymbol{X_{femur}}$: The line perpendicular to $\boldsymbol{Z_{femur}}$, and the line connecting the medial and lateral epicondyles, pointing anteriorly.
$\boldsymbol{Y_{femur}}$: The line perpendicular to both $\boldsymbol{X_{femur}}$ and $\boldsymbol{Z_{femur}}$, pointing medially.

$$\boldsymbol{Z_{femur}} = \frac{\mathbf{AFE} - \mathbf{AGT}}{|\mathbf{AFE} - \mathbf{AGT}|} \tag{13}$$

$$\boldsymbol{X_{femur}}(left) = \frac{(\mathbf{MFE} - \mathbf{LFE}) \times \boldsymbol{Z_{femur}}}{|(\mathbf{MFE} - \mathbf{LFE}) \times \boldsymbol{Z_{femur}}|} \tag{14}$$

$$\boldsymbol{X_{femur}}(right) = \frac{(\mathbf{LEF} - \mathbf{MFE}) \times \boldsymbol{Z_{femur}}}{|(\mathbf{LEF} - \mathbf{MFE}) \times \boldsymbol{Z_{femur}}|} \tag{15}$$

$$\boldsymbol{Y_{femur}} = \frac{\boldsymbol{Z_{femur}} \times \boldsymbol{X_{femur}}}{|\boldsymbol{Z_{femur}} \times \boldsymbol{X_{femur}}|} \tag{16}$$

2.1.6. Tibia

Both proximal and distal LCS are proposed on the tibiae. Anatomical landmarks of the tibia (Fig. 6):

CIE: Center of Intercondylar Eminence
TT: Tibial Tuberosity
MM: Medial Malleolus
LM: Lateral Malleolus
MA: Malleolar Average location at midpoint between **MM** and **LM**

Definition of standard anatomical axes of the tibia (Fig. 6):

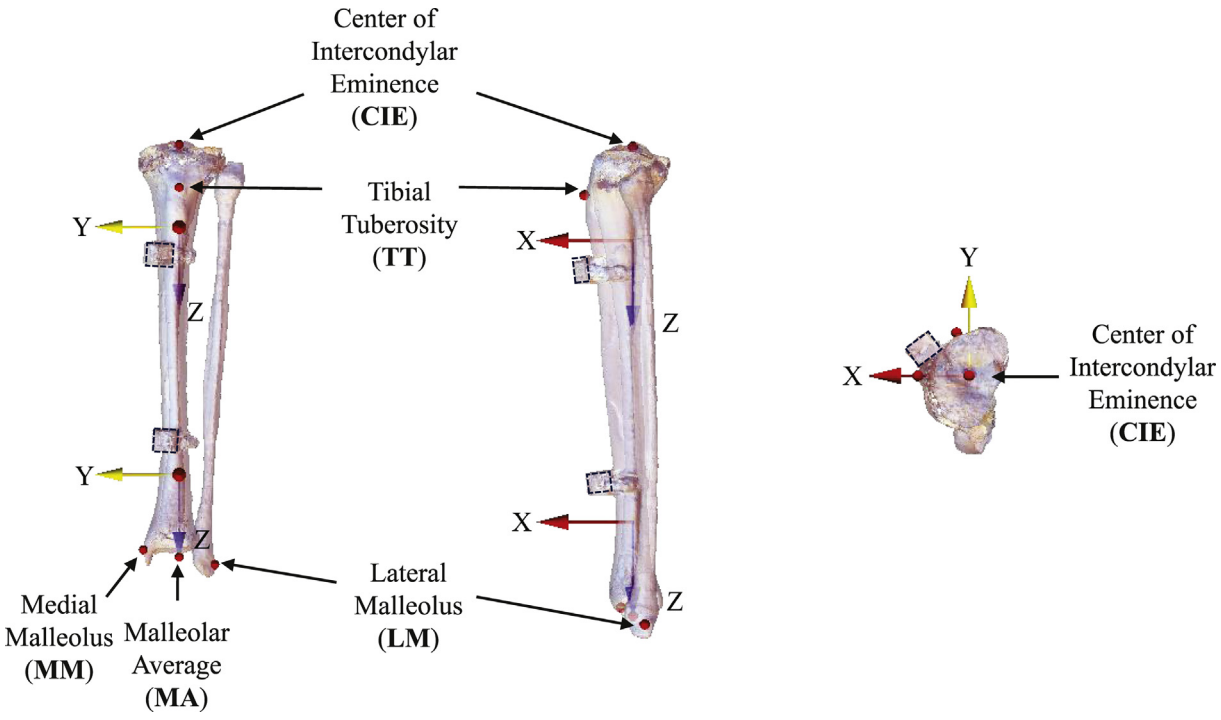

Fig. 6. Local tibia coordinate system as defined by the digitized landmarks Center of Intercondylar Eminence (**CIE**), Tibial Tuberosity (**TT**), Medial Malleolus (**MM**), and Lateral Malleolus (**LM**) and the calculated landmark Malleolar Average (**MA**). Anterior (left), lateral (center), and superior (right) views shown. Installed 6 degree-of-freedom sensor blocks are visible on the anterior surface of the distal and proximal tibial shaft.

Origin: The Proximal Tibia Origin and Distal Tibia Origin are located along $\boldsymbol{Z_{tibia}}$ at distances from **CIE** equal to 20% and 80% of the length of the tibia (ℓ_{tibia}) as defined by the difference between the Z-components of **CIE** and **MA.**

$\boldsymbol{Z_{tibia}}$: The line joining the malleolar average and the center of intercondylar eminence, pointing to the distal tibia.

$\boldsymbol{Y_{tibia}}$: The line perpendicular $\boldsymbol{Z_{tibia}}$ and the line connecting the tibial tuberosity and the center of intercondylar eminence, pointing medially.

$\boldsymbol{X_{tibia}}$**:** The line perpendicular to both $\boldsymbol{Y_{tibia}}$ and $\boldsymbol{Z_{tibia}}$, pointing anteriorly.

$$\boldsymbol{Z_{tibia}} = \frac{\mathbf{MA} - \mathbf{CIE}}{|\mathbf{MA} - \mathbf{CIE}|} \tag{17}$$

$$\boldsymbol{Y_{tibia}} = \frac{\boldsymbol{Z_{tibia}} \times (\mathbf{TT} - \mathbf{CIE})}{|\boldsymbol{Z_{tibia}} \times (\mathbf{TT} - \mathbf{CIE})|} \tag{18}$$

$$\boldsymbol{X_{tibia}} = \frac{\boldsymbol{Y_{tibia}} \times \boldsymbol{Z_{tibia}}}{|\boldsymbol{Y_{tibia}} \times \boldsymbol{Z_{tibia}}|} \tag{19}$$

3. Discussion

The LCS presented were developed using well-defined anatomical landmarks that are easily observed with medical imaging, which is a common method of defining LCS in the literature across disciplines. For example, LCS for individual vertebra have been defined by vertebral landmarks like the pedicles, endplates, and/or spinous processes for application in impact biomechanics (Danelson et al., 2015; Shaw et al., 2001; White et al., 2009), joint kinematics (Crawford and Dickman, 1997; Wu et al., 2002), and scoliosis (e.g., Kadoury et al., 2007; Stokes et al., 2009) research. The use of such landmarks allows for easy standardization of LCS across all subjects used within a single study and across different studies.

To compare ATD and PMHS data, the data must be translated from the PMHS sensor locations to skeletal locations that correspond to ATD sensor locations. Appendix II (Rudd et al., 2006; SAE, 1995) demonstrates that translation distance can have a discernible influence on sensor output. Sensor data shape and magnitude are altered when the data are translated from the proximal femur sensor to the distal femur LCS (distance: ~194 mm), but are altered less when data are translated from the distal femur sensor to the distal femur LCS (distance: ~46 mm). It follows that data translations are only appropriate where rigid body assumptions are valid. Therefore, the proposed LCS minimize, whenever reasonable, the distances required for the translation of PMHS kinematic measurements to locations relevant to both the WIAMan and other ATDs.

Although every effort was made to have the coordinate systems relate to sensor locations on ATDs, some LCS do not directly correspond to locations for which kinematic instrumentation is typically installed on existing ATDs. Although present on the WIAMan ATD, sternum, spinal, or leg accelerometers are not standard equipment on most current ATDs. Distal and proximal LCS are defined for both the femurs and tibias to minimize translation distances along the bones regardless of where the sensors are located on the ATD (e.g., the proximal femoral shaft on the WIAMan ATD or the mid femoral shaft on other ATDs). With an origin corresponding to the mid-PSIS, the pelvis LCS has the greatest deviation from the corresponding sensor location for the WIAMan (Pietsch et al., 2016) and other ATDs. However, the pelvis LCS does better approximate ATD pelvis sensor location than other published pelvis coordinate systems (e.g., Padgaonkar, 1976; Wu et al., 2002).

The LCS presently defined are the first to be appropriate and sufficient to compare PMHS response both between measurements from multiple PMHS specimens and against measurements from ATDs. Coordinate systems for each skeletal region of interest are defined based on landmarks from CT scans that can be consistently defined for both whole body and partial body PMHS specimens. The locations of the proposed LCS allow for the translation of PMHS data to ATD-relevant locations with minimal error, which will aid in the development and validation of ATDs to be used in the assessment of injury responses in impact conditions.

Acknowledgements

This work was supported under contract #N00024-13-D-6400, sponsored by the U.S. Army Research Lab in support of the Warrior Injury Assessment Manikin Program. The authors gratefully acknowledge the contributions of the WIAMan Engineering Office. The views expressed are those of the authors and do not necessarily represent the official position or policy of the U. S. Government, the Department of Defense (or its branches), or the Department of the Army.

Conflict of interest statement

The authors have no known conflict of interest related to this paper.

Appendix A. Supplementary material

Supplementary data to this article can be found online at https://doi.org/10.1016/j.jbiomech.2019.05.032.

References

Bailey, A.M., Christopher, J.J., Brozoski, F., Salzar, R.S., 2015. Post mortem human surrogate injury response of the pelvis and lower extremities to simulated underbody blast. Ann. Biomed. Eng. 43, 1907–1917.

Benoit, D.L., Ramsey, D.K., Lamontagne, M., Xu, L., Wretenberg, P., Renström, P., 2006. Effect of skin movement artifact on knee kinematics during gait and cutting motions measured in vivo. Gait Posture 24 (2), 152–164.

Chien, P.C., Parks, E.T., Eraso, F., Hartsfield, J.K., Roberts, W.E., Ofner, S., 2009. Comparison of reliability in anatomical landmark identification using two-dimensional digital cephalometrics and three-dimensional cone beam computed tomography in vivo. Dentomaxillofac. Radiol. 38, 262–273.

Crawford, N.R., Dickman, C.A., 1997. Construction of local vertebral coordinate systems using a digitizing probe. Spine 22, 559–563.

Danelson, K.A., Kemper, A.R., Mason, M.J., Tegtmeyer, M., Swiatkowski, S.A., Bolte IV, J.H., Hardy, W.N., 2015. Comparison of ATD to PMHS response in the underbody blast environment. Stapp Car Crash J. 59, 445–520.

Daniel, R.P., Irwin, A., Athey, J., Balser, J., Eichbrecht, P., Hultman, R.W., Kirkish, S., Kneisly, A., Mertz, H., Nusholtz, G. and Rouhana, S., 1995. Technical specifications of the SID-IIs dummy (No. 952735). SAE Technical Paper.

Foster, J.K., Kortge, J.O., Wolanin, M.J., 1977. Hybrid III—a biomechanically-based crash test dummy. SAE Trans., 3268–3283

Grood, E.S., Suntay, W.J., 1983. A joint coordinate system for the clinical description of three-dimensional motions: application to the knee. J. Bomech. Eng. 105 (2), 136–144.

Haffner, M., Eppinger, R., Rangarajan, N., Shams, T., Artis, M., Beach, D., 2001, June. Foundations and elements of the NHTSA Thor Alpha ATD design. In 17th ESV Conference, Paper (No. 458).

Holden, J.P., Orsini, J.A., Lohman Siegel, K., Kepple, T.M., Gerber, L.H., Stanhope, S.J., 1997. Surface movement error in shank kinematics and kinetics during gait. Gait Posture 6, 217–227.

Kadoury, S., Cheriet, F., Laporte, C., Labelle, H., 2007. A versatile 3D reconstruction system of the spine and pelvis for clinical assessment of spinal deformities. Med. Biol. Eng. Comput. 45, 591–602.

Kerrigan, J.R., Crandall, J.R., Deng, B., 2008. A comparative analysis of the pedestrian injury risk predicted by mechanical impactors and post mortem human surrogates. Stapp Car Crash J. 52, 527–567.

Padgaonkar, A.J., 1976. Validation study of a three-dimensional crash victim simulator for pedestrian-vehicle impact. Mechanical engineering (Biomechanics). Detroit, Wayne State University. Doctor of Philosophy.

Pennock, G.R., Clark, K.J., 1990. An anatomy-based coordinate system for the description of the kinematic displacements in the human knee. J. Biomech. 23, 1209–1218.

Pietsch, H.A., Bosch, K.E., Weyland, D.R., Spratley, E.M., Henderson, K.A., Salzar, R.S., Smith, T.A., Sagara, B.M., Demetropoulos, C.K., Dooley, C.J., Merkle, A.C., 2016. Evaluation of WIAMan technology demonstrator biofidelity relative to sub-injurious PMHS response in simulated under-body blast events. Stapp Car Crash J. 60, 199–246.

Rudd, R., Kerrigan, J., Crandall, J., Arregui, C., 2006. Kinematic analysis of head/neck motion in pedestrian-vehicle collisions using 6-degree-of-freedom instrumentation cubes, 2006 SAE World congress.

SAE J211 "Instrumentation for Impact Test," SAE J211/1 MAR 1995, 1995 SAE Handbook Volume 4 - On-Highway Vehicles & Off-Highway Machinery, Society of Automotive Engineers, Warrendale, PA. 1995.

Shaw, C., Kent, R., Sieveka, E., Crandall, J., 2001. Spinal kinematics of restrained occupants in frontal impacts. In: IRCOBI Conference on the Biomechanics of Impact.

Stagni, R., Leardini, A., Cappozzo, A., Benedetti, M.G., Cappello, A., 2000. Effects of hip joint centre mislocation on gait analysis results. J. Biomech. 33 (11), 1479–1487.

Stokes, I.A.F., 1994. Scoliosis research society working group on 3-D terminology of spinal deformity (three-dimensional terminology of spinal deformity). Spine 19, 236–248.

Stokes, I.A., Sangole, A.P., Aubin, C.E., 2009. Classification of scoliosis deformity 3-d spinal shape by cluster analysis. Spine 34, 584–590.

White, N.A., Begeman, P.C., Hardy, W.N., Yang, K.H., Ono, K., Sato, F., Kamiji, K., Yasuki, T., Bey, M.J., 2009. Investigation of upper body and cervical spine kinematics of post mortem human subjects (PMHS) during low-speed, rear-end impacts (No. 2009-01-0387). SAE Technical Paper.

Wu, G., Siegler, S., Allard, P., Kirtley, C., Leardini, A., Rosenbaum, D., Whittle, M., D D'Lima, D., Cristofolini, L., Witte, H., Schmid, O., 2002. ISB recommendation on definitions of joint coordinate system of various joints for the reporting of human joint motion—part I: ankle, hip, and spine. J. Biomech. 35, 543–548.

Yoshioka, Y., Siu, D.W., Cooke, T.D., 1987. The anatomy and functional axes of the femur. J. Bone Joint Surg. 69A, 873–880.